Simulation of defect evolution in irradiated materials: Role of intracascade clustering and correlated recombination

C. J. Ortiz* and M. J. Caturla
Departamento de Física Aplicada, Universidad de Alicante, 03690 San Vicente del Raspeig, Spain
(Received 22 December 2006; revised manuscript received 24 February 2007; published 8 May 2007)

The evolution of damage produced by collision cascades in Fe is studied using both kinetic Monte Carlo (kMC) and rate theory (RT) approaches. The initial damage distribution is obtained from molecular-dynamics simulations of 30 keV recoils in Fe. An isochronal annealing is simulated to identify the different thermally activated mechanisms that govern defect evolution. When clusters form during collision cascades, kMC simulations show that additional recovery peaks should be expected, in comparison to recovery curves obtained under electron irradiation conditions. Detailed kMC and RT simulations reveal that some of these recovery peaks are due to correlated recombinations at low temperature between defects. In particular, we show that under cascade-damage conditions it is possible to observe correlated recombinations between vacancies and self-interstitial clusters. These correlated recombinations cannot be reproduced with a RT model, and therefore kMC and RT differ at low temperature. However, for the conditions presented here, the contribution of correlated recombination is very small and therefore no significant differences are observed at high temperatures between these two models.

DOI: 10.1103/PhysRevB.75.184101 PACS number(s): 61.80.Az, 61.72.Cc, 61.72.Ji, 66.30.−h

I. INTRODUCTION

The displacement damage produced in metals by high-energy particles such as electrons, protons, ions, or neutrons can result in significantly different defect distributions. Typically, collisions with light particles such as electrons produce Frenkel pairs,[1] i.e., pairs of spatially separated self-interstitials and vacancies. In contrast, particles such as heavy ions or neutrons create collision cascades which yield not only Frenkel pairs but also interstitial and vacancy clusters,[2,3] resulting in a heterogeneous defect distribution. Depending on temperature, point defects produced during irradiation can migrate and either recombine or agglomerate to form larger defect clusters. These defects can alter the microstructure and thus, the mechanical properties of the material. Therefore, in view of providing models able to predict the long-term performance of materials under irradiation, and in particular metals, considerable effort is being devoted to calculate the energetic properties of defects[4,5] and to understand the physical mechanisms governing their nucleation and growth.[6–10]

The evolution of defects upon irradiation and annealing is by nature a multiscale phenomenon. Indeed, displacement cascades take place in volumes and times of the order of nm^3 and ps, respectively, whereas defects diffuse for hours or even years over large distances. Therefore, the study of defect evolution requires a multilevel analysis which spans from atomistic to continuum approaches.[11] Molecular dynamics (MD) is nowadays a widely used simulation technique for studying the formation of defects generated by atomic collision cascades in materials.[2,3] Given an interatomic potential, the Newton equations of motion of each atom are numerically solved. It is therefore a powerful tool to investigate displacement cascades. However, at temperatures at which defects produced in the cascade are mobile, diffusion gives rise to interactions that extend over macroscopic length and time scales, which are computationally unaccessible to MD simulations. A simulation tool able to simulate the long-time evolution of displacement cascade is thus necessary. During the past decade, kinetic Monte Carlo (kMC) has become a common modeling technique to simulate the ensuing evolution of defects produced during irradiation.[6–8] kMC follows the evolution of an ensemble of defects in time, given the type of atomistic processes those defects can undergo and given the probability for each event to occur. Therefore, it requires previous knowledge of defects created during irradiation, their mobilities as well as their energetic properties, i.e., binding energies of clusters. One of the main advantages of this method is that it retains the atomic nature of processes, and therefore, can treat difficult issues such as spatial correlations or inhomogeneities induced by displacement cascades. However, in practice, kMC simulations are limited to small volumes (up to 1 μm cube, depending on the conditions) and become computationally expensive when the irradiation dose is high and/or when time scales of the order of nuclear reactor lifetime should be explored. This limitation can be circumvented by using rate theory (RT) as an alternative. Within this approach based on the mean-field approximation, the diffusion of defects is modeled through a set of diffusion-reaction rate equations, whereas the nucleation and/or growth of clusters is described by the master equation. The small computational resources required by RT approach make it attractive and allow us to explore the evolution of defects over large time scales and over large distances, close to those achieved experimentally. Different research teams[12–17] have used this approach to study the nucleation and growth of defects in various materials over the years. Recently, Rottler *et al.*[18] used the RT formalism to investigate point defect dynamics in metals and showed that when defects are homogeneously distributed, kMC and RT models are in near perfect agreement. However, one of the basic assumptions in the mean-field approximation is that defect production is uniform in time and space at some appropriate value. Therefore, under

continuous irradiation conditions, the RT approach does not account for the stochastic effects caused by the random nature of the cascade initiation. Indeed, point defects and clusters are generated randomly in time and space during irradiation. In a rigorous theoretical investigation, Semenov and Woo[19,20] showed that under typical cascade-damage conditions, cascade-induced fluctuations play a much more important role than fluctuations due to the random point defect jumps. Hence, the conventional RT approach is not adequate to describe the evolution of the microstruture under continuous irradiation and must be reformulated beyond the mean-field approximation and such that the probabilistic nature of cascade initiation is taken into account, as it was done by Semenov and Woo.[20,21] Also, when complex mechanisms have to be considered, results obtained by RT models can deviate from those obtained by kMC. For instance, in a recent work, Fu *et al.*[9] successfully reproduced resistivity recovery experiments of electron-irradiated iron from Takaki *et al.*[1] using a kMC model with input parameters from *ab initio* calculations. Using the same input parameters, Dalla Torre *et al.*[22] showed that due to the lack of spatial correlations in the mean-field approach, the results from RT strongly differ from those obtained by kMC. In particular, the authors evidenced that RT is unable to predict stage I_{D2}, responsible for the recombination of correlated *I-V* Frenkel pairs at $T=107.5$ K. On the other hand, the authors also showed that RT models can achieve a quantitative agreement with kMC results when the exact defect population after stage I_E, corresponding to the uncorrelated recombination of *I-V* due to the free migration of *I* at $T \simeq 140$ K, is first calculated by kMC and used as initial conditions in the RT model. This multiscale approach ensures that correlated recombinations occurring at the beginning of annealing are taken into account in the rate equations.

Under most irradiation conditions other than electron irradiation, the localized damage areas produced result not only in the formation of well separated Frenkel pairs but also in the formation of clusters of vacancies and self-interstitials just a few picoseconds after the initial collision. Consequently, the spatial and size distributions of defects produced during, e.g., ion irradiation are much more complex than those generated by an electron irradiation. It is thus expected that the ensuing evolution of defects follows a more complex kinetics as well. Thus, under these conditions, it is not clear how reliable RT models are as compared to kMC to study the evolution of defects in irradiated materials. To further elucidate this question, in the present contribution, we propose to study the evolution of defects produced in collision cascades in iron during a subsequent isochronal annealing, using kMC and RT approaches. In particular, the aim of the present investigation is to shed light on the role of initial intracascade clustering and correlated recombinations in the evolution of the cluster and point defect populations. In Secs. II and III, kMC and RT formalisms are briefly described. The main atomistic processes governing interaction between defects in iron as well as the parameters used in the model are given in Sec. IV. In Sec. V, we compare kMC and RT results for an isochronal annealing of defects created by displacement cascades produced by a 30 keV Fe irradiation in Fe. Simulation results obtained with the kMC and RT models are then discussed in Sec. VI.

II. KINETIC MONTE CARLO MODEL

The name kinetic Monte Carlo is often used to describe different types of algorithms that involve evolution in time. It follows the evolution of a set of objects, given the type of events those objects can perform and the probability for each event to occur. The first simulations using this technique date back to the middle 1960s to early 1970s,[23,24] but it is in recent years when it has been more commonly used in the field of radiation effects. In the case of radiation in solids, the objects of interest are the defects produced during irradiation, that is, vacancies, self-interstitials, and their clusters. In this model, defects are assumed to be pointlike, i.e., their detailed atomic configuration is ignored. The events these objects—defects here—can perform are diffusion jumps, dissociation from a cluster, or interaction between different defects. The probabilities of these events are given by their migration and binding energies. For example, the probability of a defect of type *i* undergoing a migration event is proportional to the jump frequency given by

$$\Gamma_m^i = \Gamma_0^i \exp\left(-\frac{E_m^i}{kT}\right), \tag{1}$$

where Γ_0^i is the attempt frequency, E_m^i is the migration energy for that particular defect, k is Boltzmann's constant, and T is the absolute temperature. When a migration event is selected, the object is moved a distance δ (the jump distance), which is often selected between the first and second nearest neighbors. After a defect undergoes a jump, it can spontaneously recombine or aggregate to another defect whenever their mutual distance is smaller than a critical distance called the capture distance.

The probability of a defect of type *i* to dissociate from a cluster is related to the dissociation frequency:

$$\Gamma_d^i = \Gamma_0^i \exp\left(-\frac{E_m^i + E_b^i}{kT}\right), \tag{2}$$

where E_b^i is the binding energy of the defect to the cluster. In general, this energy depends on the size of the cluster.

To simulate the evolution of the system, the kMC algorithm proceeds by selecting an event from all the possible ones. First, the cumulative function R_i is defined as follows:

$$R_i = \sum_{j=1}^{i} \Gamma_j N_j, \tag{3}$$

for $i=1,\ldots,N$ where N is the total number of transitions. The probability of an event i is Γ_i and the number of objects that can undergo that event is N_i. Then, a random number $\alpha \in [0,1]$ is chosen and the event i to carry out is selected such that $R_{i-1} < \alpha R_N \leqslant R_i$, R_N being the total rate for all events. Once the event has been selected, an object is chosen randomly between 0 and N_i from all those that can undergo that event. The time of the simulation is then increased by Δt such that

$$\Delta t = \frac{-\log \xi}{R_N}, \tag{4}$$

where ξ is a random number between 0 and 1, that is used to obtain a Poisson distribution of the time.

The initial conditions of the simulation are the (x,y,z) coordinates of those defects produced by the irradiation as well as their type. This information can be obtained, for example, by MD simulations.

III. RATE THEORY FORMALISM

Alternatively, the atomistic processes described by the kMC model can be described within a rate equation formalism. In this framework, point defect and cluster kinetics are assumed to follow the kinetic law of mass action derived by Bronsted.[25] As in the kMC model, reactions between point defects and clusters are supposed to occur via binary reactions of the type

$$A + B \underset{k_C^-}{\overset{k_{A+B}^+}{\rightleftharpoons}} C. \tag{5}$$

The symbols k_{A+B}^+ and k_C^- stand for the capture and dissociation rate constants of the reaction, respectively. Assuming that the reaction rates follow the kinetic law of mass action, the generation-recombination (GR) rate corresponding to reaction (5), i.e., the net difference between the generation and the loss rate, can be written as

$$\mathrm{GR}_{A+B} = k_{A+B}^+ C_A C_B - k_C^- C_C. \tag{6}$$

Then, according to the mass conservation, it follows that the time evolution of the mean concentration of, e.g., species B is governed by the partial differential equation (PDE):

$$\frac{\partial C_B}{\partial t} = -\operatorname{div} \vec{J}_B - \mathrm{GR}_{A+B} = D_B \Delta C_B - (k_{A+B}^+ C_A C_B - k_C^- C_C), \tag{7}$$

in which it was assumed that atoms B diffuse with a constant diffusion coefficient D_B. Equations for species A and C can be derived following the same methodology. As we can see, within this formalism, the time evolution of the system is governed by a set of coupled nonlinear PDEs. However, the kinetic law of mass action only gives the structure of kinetic equations but does not give any information about the rate constants, namely, k_{A+B}^+ and k_C^-. These constants, which determine the velocity of forward and backward reactions, must be obtained from kinetic theories. This point will be addressed in the following sections.

A. Forward constant

A convenient way to obtain the rate constant in the forward direction is the theory of diffusion-limited reactions. First presented by von Smoluchowski[26] in 1917 for the coagulation in colloidal solutions and derived later by Waite[27] on a statistical basis, the forward rate constant of diffusion-limited reactions $A+B \rightarrow C$ is determined mainly by the diffusion of the reactants toward each other and is written as follows:

$$k_{A+B}^+ \simeq 4\pi(r_A + r_B)(D_A + D_B), \tag{8}$$

where D_A and D_B are the diffusion coefficients of the reacting species A and B, respectively. These diffusion coefficients are related to the jump frequencies used in kMC [see Eq. (1)] as $D=\Gamma_m^i \delta^2/2d$, where d is the dimension for diffusion. Similar to the kMC approach, the reaction is assumed to take place spontaneously when the reactants approach one another to within a critical distance $r_{AB}=r_A+r_B$. At this point, it is important to note that the constant in the form (8) was derived by Waite[27] in the particular case of particles randomly distributed with respect to one another, i.e., conditions in which correlation effects do not play any role. Since it is expected that under irradiation conditions defects might occupy closely correlated sites, Waite[28] and later Peak and Corbett[29] discussed possible extensions to include spatial correlation effects within the Waite formalism presented in Ref. 27. However, solutions given in both attempts strongly depend on the assumption that is made on the initial spatial distribution of defects. Hence, in most cases the theory of diffusion-limited reactions can only account for the regime of uncorrelated recombinations, which rate constant is given by Eq. (8).

B. Backward constant

Having quantified the formation rate constant of reaction (5), we need to derive also the corresponding backward rate constant, i.e., the frequency at which the inverse reaction $C \rightarrow A+B$ occurs. To do so, we consider the fact that in steady state, formation and dissociation rates must be equal, i.e., $\mathrm{GR}_{A+B}=0$. This leads to the well-known law of mass action:

$$\frac{k_C^-}{k_{A+B}^+} = \left.\frac{C_A C_B}{C_C}\right|_{eq}. \tag{9}$$

Alternatively, this expression can be written in terms of the energetics of defects, which enables us to express the dissociation frequency k_C^- as follows:

$$k_C^- = k_{A+B}^+ N_s \exp\left(-\frac{G_A^f + G_B^f - G_C^f}{k_B T}\right), \tag{10}$$

where G_A^f, G_B^f, and G_C^f are the Gibbs free formation energies of species A, B, and C, respectively. These energies are related to the binding energy E_b^i used in kMC simulations by $E_b^i = G_A^f + G_B^f - G_C^f$. N_s is the number of available sites, which is assumed to be the same for all defects considered here.

IV. POINT DEFECT AND CLUSTER KINETICS IN IRRADIATED Fe

In order to illuminate the role of intracascade clustering and correlated recombinations in the evolution of defects in irradiated materials, we selected to study the case of cascade damage in iron. In this section, we provide the various atomistic processes describing the kinetics of point defects and

clusters in iron. The mobile species considered in this model are single vacancies, single self-interstitials, and di-interstitials. The experimental observations of Takaki *et al.*[1] and recent theoretical calculations of Fu *et al.*[5] have shown that mobile di-interstitial clusters must be considered to reproduce some of the features observed in irradiated Fe. For simplicity, larger self-interstitial and vacancy clusters are considered immobile in this model. Based on these assumptions, the reactions that govern the evolution of point defects and clusters are the following.

(1) Recombination between self-interstitials and vacancies:

$$I + V \rightleftharpoons 0, \tag{11}$$

where I denotes self-interstitials and V vacancies. This reaction is characterized by the forward constant k^+_{I+V}.

(2) Formation of vacancy clusters:

$$V_n + V \rightleftharpoons V_{n+1}, \tag{12}$$

where V_n and V_{n+1} stand for vacancy clusters comprising n and $n+1$ vacancies, respectively. The aggregation of vacancies to clusters of n vacancies and dissolution of V_{n+1} clusters occur with rates β^+_n and β^-_{n+1}, respectively.

(3) Formation of self-interstitial clusters:

$$I_n + I \rightleftharpoons I_{n+1}, \tag{13}$$

in which I_n and I_{n+1} denote clusters containing n and $n+1$ self-interstitials, respectively. Formation and dissociation of I_{n+1} clusters occur with rates γ^+_n and γ^-_{n+1}, respectively.

(4) Formation of self-interstitial clusters by agglomeration of di-interstitials:

$$I_n + I_2 \rightleftharpoons I_{n+2}. \tag{14}$$

According to this reaction, interstitial clusters can also form by agglomeration of mobile di-interstitials. The corresponding formation and dissociation rates are ω^+_n and ω^-_{n+2}, respectively.

(5) Recombination of vacancies with self-interstitial clusters:

$$I_n + V \rightarrow I_{n-1}. \tag{15}$$

The loss rate of vacancies by recombination with I_n clusters is $k^+_{I_n+V}$. Since this reaction is considered to be irreversible due to its high binding energy, the reverse reaction rate does not need to be defined here.

Recombination of self-interstitials with vacancy clusters:

$$V_n + I \rightarrow V_{n-1}, \tag{16}$$

which occurs with rate $k^+_{V_n+I}$. The emission of a self-interstitial from a vacancy cluster is neglected because of the high binding energy involved in the reaction.

At this point, we want to stress that the purpose of this work is not to develop a physical model able to predict in detail the kinetics of defects in irradiated iron but to underline the role of intracascade clustering in the evolution of defects in materials under collision cascade conditions. Therefore, the assumptions made above are sufficient to capture the main characteristics of defect evolution in irradiated iron. In particular, we shall see that even though migration of large clusters is not taken into consideration, the inclusion of intracascade clustering leads to surprisingly different features of the defect-population evolution, in comparison to electron irradiation conditions.

A. Rate equations

Following the formalism introduced in Sec. III and according to the model depicted above, we shall now derive the continuity equations that govern the kinetics of point defects and clusters in irradiated iron. Taking into account the different reactions involving self-interstitials, the mean concentration of I evolves according to the following PDE:

$$\frac{\partial C_I}{\partial t} = D_I \Delta C_I - \mathrm{GR}_{I+V} - \mathrm{GR}_{I_n+I} + \mathrm{GR}_{I_2+V} - \mathrm{GR}_{V_n+I}. \tag{17}$$

The first term on the right-hand side (RHS) of the equation above is the Fickian term accounting for diffusion of self-interstitials. The next term, GR_{I+V}, results from the mutual annihilation of self-interstitials and vacancies in the bulk corresponding to reaction (11). Agglomeration of self-interstitials into interstitial clusters is described by the term GR_{I_n+I} [Eq. (13)]. The term GR_{I_2+V} accounts for the generation of self-interstitials by recombination of di-interstitials with vacancies, which is a particular case of reaction (15). Finally, the last term takes into account the annihilation of interstitials at vacancy clusters, corresponding to reaction (16). Now, let us specify each of the GR terms present in Eq. (17). As it can be easily demonstrated, the recombination rate of I and V can be obtained from steady-state considerations and can be expressed in terms of the capture constant k^+_{I+V} and the equilibrium concentrations of point defects so that GR_{I+V} can be written in the well-known form

$$\mathrm{GR}_{I+V} = k^+_{I+V}(C_I C_V - C_I^{eq} C_V^{eq}), \tag{18}$$

where C_I^{eq} and C_V^{eq} are the concentrations of self-interstitials and vacancies at thermodynamical equilibrium, respectively. To determine the generation-recombination term GR_{I_n+I}, we must consider all possible reactions between self-interstitials and I_n clusters of all sizes. This leads to the following expression for GR_{I_n+I}:

$$\mathrm{GR}_{I_n+I} = 2(\gamma^+_1 C_I^2 - \gamma^-_2 C_{I_2}) + \sum_{n \geqslant 2} (\gamma^+_n C_{I_n} C_I - \gamma^-_{n+1} C_{I_{n+1}}). \tag{19}$$

The factor 2 in front of the first term in the equation above comes from the fact that the formation or the dissociation of a di-interstitial removes or releases two self-interstitials, respectively. The generation rate of interstitials resulting from the reaction of di-interstitials with vacancies is simply given by

$$\mathrm{GR}_{I_2+V} = k^+_{I_2+V} C_{I_2} C_V. \tag{20}$$

Finally, the annihilation rate of interstitials at vacancy clusters is given by the following sum:

$$\mathrm{GR}_{V_n+I} = \sum_{n\geqslant 2} k^+_{V_n+I} C_{V_n} C_I. \tag{21}$$

In order to derive the continuity equation for vacancies, one proceeds in a similar way and easily gets

$$\frac{\partial C_V}{\partial t} = D_V \Delta C_V - \mathrm{GR}_{I+V} - \mathrm{GR}_{V_n+V} - \mathrm{GR}_{I_n+V} + \mathrm{GR}_{V_2+I}. \tag{22}$$

The term GR_{I+V}, previously calculated for the bulk recombination of self-interstitials, is given by Eq. (18). The next term corresponds to the formation-dissociation of V_n clusters of all sizes and is given by an expression similar to Eq. (19). The next GR term of Eq. (22) accounts for the loss of vacancies by recombination with interstitial clusters. The last term appearing on the RHS of Eq. (22) accounts for the formation of a vacancy when a divacancy recombines with a self-interstitial. As for the case of self-interstitials, the expression of these GR terms can be derived in a straightforward way and will not be given here. Following the same procedure, one can derive the diffusion-reaction equation governing the concentration of mobile di-interstitials:

$$\frac{\partial C_{I_2}}{\partial t} = D_{I_2} \Delta C_{I_2} - \mathrm{GR}_{I_n+I_2} - \mathrm{GR}_{I_2+V} + \mathrm{GR}_{I+I}. \tag{23}$$

The first GR term on the RHS of Eq. (23) accounts for the agglomeration of di-interstitials. GR_{I_2+V} term accounts for the annihilation of di-interstitials with vacancies. The last term accounts for the formation and dissociation of I_2 clusters.

Now that the continuity equations for mobile defects have been derived, we must obtain the equations governing the evolution of immobile I_n and V_n clusters. According to reactions (13)–(15), the concentration of interstitial clusters I_n—with a discrete number of atoms n—evolves according to

$$\begin{aligned}\frac{\partial C_{I_n}}{\partial t} &= \gamma^+_{n-1} C_I C_{I_{n-1}} - \gamma^-_n C_{I_n} - \gamma^+_n C_I C_{I_n} + \gamma^-_{n+1} C_{I_{n+1}} \\ &+ \omega^+_{n-2} C_{I_2} C_{I_{n-2}} - \omega^-_n C_{I_n} - \omega^+_n C_{I_2} C_{I_n} + \omega^-_{n+2} C_{I_{n+2}} \\ &- k^+_{I_n+V} C_V C_{I_n} + k^+_{I_{n+1}+V} C_V C_{I_{n+1}}.\end{aligned} \tag{24}$$

Similarly, a master equation can be derived for vacancy clusters containing n vacancies:

$$\begin{aligned}\frac{\partial C_{V_n}}{\partial t} &= \beta^+_{n-1} C_V C_{V_{n-1}} - \beta^-_n C_{V_n} - \beta^+_n C_V C_{V_n} + \beta^-_{n+1} C_{V_{n+1}} \\ &- k^+_{V_n+I} C_I C_{V_n} + k^+_{V_{n+1}+I} C_I C_{V_{n+1}}.\end{aligned} \tag{25}$$

Rate constants of reactions (11)–(16) were calculated using expressions (8) and (10) and the same parameters that were used in the kMC model to calculate event probabilities. These parameters are given in the following sections.

B. Energetic properties of defects in Fe

Equations (1) and (2), defining the probabilities of migration and dissociation in the kMC model, and Eqs. (8)–(10), describing the forward and backward rates of reaction in the RT model, show that the defect-population evolution is determined by the energetic properties of defects. In this work, we used the migration and binding energies of defects calculated by Fu *et al.*[5,9] in the framework of the density-functional theory. For the formation energies of the mono-interstitial and monovacancy, the authors found 3.77 and 2.07 eV, respectively. Table I summarizes the binding energies obtained by Fu *et al.*[9] for small interstitial and vacancy clusters. For larger clusters, an extrapolation law was used to calculate their binding energies, as it is done in other works.[9,10,30] According to *ab initio* calculations from Ref. 5, migration energies of 0.34, 0.67, and 0.42 eV were used for the monointerstitial, monovacancy, and di-interstitial clusters, respectively.

TABLE I. Binding energies of small interstitial and vacancy clusters in Fe according to Ref. 9.

	I_n (eV)	V_n (eV)
$n=2$	0.80	0.30
$n=3$	0.92	0.37
$n=4$	1.64	0.62

C. Capture radii of defects

As we have seen in Secs. II and III, in the kMC and RT models it is assumed that a reaction between two defects takes place spontaneously if the defects are located within a critical distance which is the sum of their capture radii. This parameter thus defines the distance at which defects interact with each other. In this work, the interaction volume of a defect is approximated by a sphere of radius r, in the kMC as well as in the RT model. This is certainly a simplistic approach from the atomic-level point of view. However, this assumption is widely accepted and used in other kMC and RT models.[7,8,22,30] As it is observed experimentally, in our model, interstitial-type defects develop a larger strain field than vacancy-type defects. This is achieved by introducing a bias factor $Z=1.15$ in the capture radii of interstitial defects. This value is deduced from experimental results and corresponds to a fairly common choice.[7,8,30] The capture radii used in this work account then for the volume occupied by the defect and the interaction range corresponding to the strain field and are given by

$$r_{V_n} = \left(\frac{3n\Omega}{4\pi}\right)^{1/3} + r_0, \tag{26}$$

$$r_{I_n} = Z\left[\left(\frac{3n\Omega}{4\pi}\right)^{1/3} + r_0\right], \tag{27}$$

where r_{V_n} is the capture radius of a vacancy cluster containing n vacancies and r_{I_n} is the capture radius of an interstitial cluster comprising n interstitials. Ω is the atomic volume and Z the bias factor for interstitial defects. In Eqs. (26) and (27), $r_0=3.3$ Å, which was calculated such that the I-V recombi-

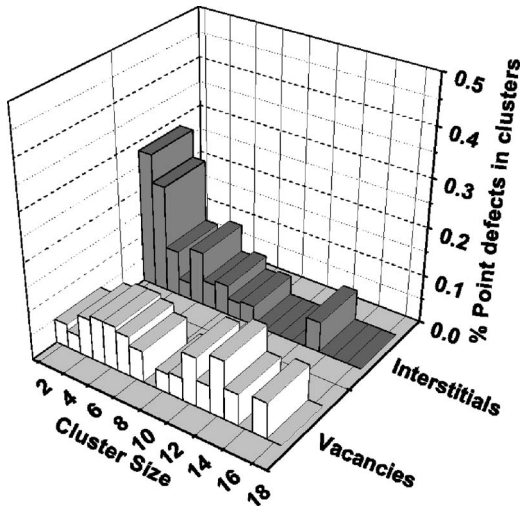

FIG. 1. Size distribution of interstitial and vacancy clusters formed by intracascade clustering for a 30 keV Fe irradiation in Fe.

nation distance is 3.3 lattice parameters, in agreement with experimental results[31] and simulation works.[10,32] The same approach was used in other works.[9]

V. EVOLUTION OF DEFECTS IN ION-IRRADIATED Fe: COMPARISON BETWEEN KMC AND RT

In the present work, we have selected as an example of damage evolution the case of isochronal annealing of defects created by a 30 keV Fe irradiation in Fe. As in the recovery experiment on electron-irradiated Fe, the temperature is raised from 77 up to 800 K with isochronal steps of $\Delta t = 300$ s and temperature intervals such that $\Delta T/T = 0.03$. The defects produced by the 30 keV Fe irradiation were calculated by means of MD simulations. The interatomic potential developed by Ackland *et al.*[33] was used to reproduce the interaction between atoms in the Fe lattice. Although new potentials developed recently[34,35] better reproduce Fe properties, the choice of the potential is secondary here since the aim is to compare the evolution obtained by two different methods starting from the same initial damage distribution. Moreover, calculations performed using results obtained with the interatomic potential developed by Dudarev and Derlet[35] of 30 keV cascades in Fe do not show significant differences with those presented here. The average number of Frenkel pairs produced during the irradiation was obtained on the basis of ten cascade simulations. The Frenkel pairs were identified using the Wigner-Seitz cell method. Following this procedure, we found that on average, 75 stable Frenkel pairs are produced per cascade, which corresponds approximately to a 20% efficiency compared to the Norgett-Robinson-Torrens formula, and in agreement with previous calculations.[32] Considering the capture radii given in Sec. IV, point defects were then grouped into interstitial and vacancy clusters. As a result, the final number of Frenkel pairs produced in a 30 keV Fe cascade after recombination and clustering was found to be 22. In Fig. 1, we reported the predicted size distribution for interstitial and vacancy clusters resulting from the 30 keV Fe irradiation in Fe. As one can see, after irradiation most of the point defects generated by the collision cascade are agglomerated into clusters. In particular, MD simulations show that about 50% of the vacancy clusters that are created during irradiation contain less than seven vacancies.

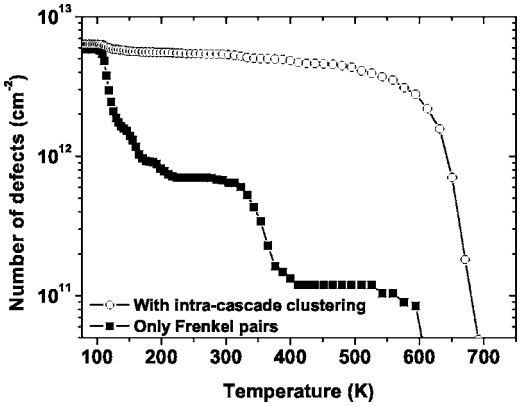

FIG. 2. Evolution of the total number of defects during isochronal annealing obtained by kMC calculations for electron (■) and 30 keV Fe (○) irradiations for a dose of 10^{-6} dpa.

To simulate the evolution of these defects with the kMC model during the isochronal annealing defined above, the position and size of each defect obtained by MD simulations were retained and used as initial conditions. The kMC code BIGMAC (Ref. 36) was used for the calculations presented here.

First, we examine the evolution of the damage created by an ion irradiation for a total dose of 10^{-6} dpa (dpa denotes displacements per atom). This corresponds approximately to a *I-V* pair concentration of 10^{17} cm^{-3}. In Fig. 2, we reported as a function of temperature the evolution of the total number of point defects predicted by kMC calculations, without discriminating between free point defects and those in clusters. For comparison, and in order to clearly evidence the effect of intracascade clustering, we also reported kMC results obtained for an electron irradiation, i.e., when only isolated Frenkel pairs are produced. As expected, the results obtained with the two initial conditions strongly differ, qualitatively as well as quantitatively. When only Frenkel pairs are considered, the kMC model predicts that defects highly recombine at low temperature. This is expected since point defects are free to migrate, which favors the rate encounter of reaction. This result is in agreement with kMC calculations performed by Fu *et al.*[9] In contrast, in the case of the 30 keV Fe irradiation, the total number of defects slowly decreases with temperature up to $T \approx 500$ K. This is expected since most point defects are immobilized into clusters after irradiation, as shown in Fig. 1. Therefore, at low temperature, only a small amount of point defects can migrate and recombine, resulting in a small decrease in the defect population. At higher temperatures, defect population decays rapidly, indicating that clusters dissolve, releasing point defects, which in turn, diffuse and annihilate.

The derivative of the total number of defects with temperature for these two cases is shown in Fig. 3. These curves evidence the different recombination mechanisms that take place during isochronal annealing. Clearly, the two initial

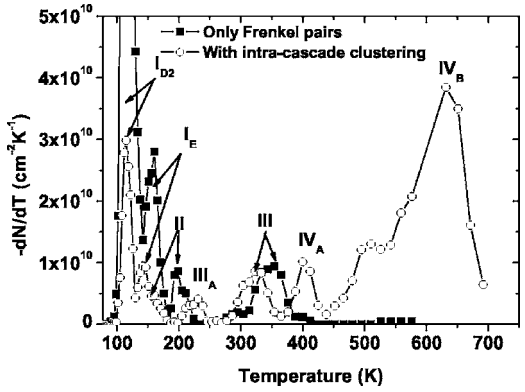

FIG. 3. Recovery stages predicted by kMC for electron (■) and 30 keV Fe (○) irradiations for a dose of 10^{-6} dpa.

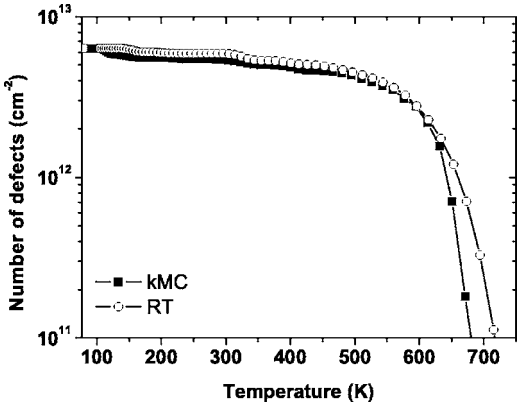

FIG. 4. Evolution of the total number of defects during isochronal annealing predicted by kMC (■) and RT (○) models for a 30 keV Fe irradiation for a dose of 10^{-6} dpa.

conditions lead to very different recovery curves. In the case where only Frenkel pairs are created, our kMC model predicts the same recovery stages reported by Takaki *et al.*[1] and Fu *et al.*[9] for electron-irradiated Fe. These peaks are the so-called stages I_{D2}, I_E, II, and III, related to the recombination of correlated *I-V* pairs by free migration of the interstitial, the recombination of *I* and *V* belonging to different Frenkel pairs by migration of *I*, and the migration of di-interstitials and vacancies, respectively. These results thus provide a validation of our model. On the other hand, when intracascade clustering occurs during irradiation, the recovery curve exhibits a more complex structure. kMC calculations show that stages I_{D2} and I_E are still present in the recovery curves, though their intensity is significantly lower than in the case of electron irradiation, as can be seen in Fig. 3. This is due to the fact that most interstitials and vacancies are immobilized into clusters after the 30 keV Fe irradiation (see Fig. 1). Therefore, correlated and uncorrelated *I-V* recombinations are less effective when irradiation generates intracascade clustering than in electron irradiation conditions. This is in agreement with experimental results of Matsui *et al.*[37] who observed that the fractional recovery of stage I is much smaller in the case of neutron irradiation compared to electron irradiation. Stage II can also be seen in the recovery curve obtained with intracascade clustering, however, shifted toward lower temperatures and even merging with that of stage I_E. This shift is due to a dose effect. Indeed, Fig. 1 shows that a large amount of di-interstitials is formed during the cascade, in comparison to electron irradiation. In addition to the stages expected under electron irradiation, the kMC model predicts the presence of three new recovery peaks, centered at $T=231$ and 400 K and one broadening from 450 to 700 K. Clearly, these new peaks are related to the initial formation of clusters in the cascade. For convenience and in order to be consistent with the nomenclature used by Takaki *et al.*,[1] in the following we will refer to these recovery peaks as III_A, IV_A, and IV_B, respectively. Their origin will be discussed in the next section. Thus, Figs. 2 and 3 clearly evidence that irradiation conditions strongly influence the subsequent kinetics of defects. Therefore, to simulate the evolution of damage caused by displacement cascades, it is crucial to take into account the initial size distribution of clusters formed during irradiation.

At this point, we want to emphasize that the defect recovery curves obtained here depend on the assumptions made in the kinetic model used to predict defect evolution. Indeed, in this study we assumed that vacancy and $I_{n\geqslant 3}$ clusters are not mobile and neglected the presence of trapping impurities such as carbon. However, it is important to note that additional kMC simulations (not shown here) taking into account the mobility of V_2, V_3, and V_4 clusters showed very similar results to those obtained here, i.e., assuming that vacancy clusters are immobile. Thus, the assumption made on the mobility of vacancy clusters does not change the conclusions drawn in the present work.

Next, RT calculations are compared to kMC results for cascade-damage conditions. Since in the RT approach only the mean concentration of defects can be followed, RT calculations were performed using as initial conditions the detailed concentrations of *I*, *V*, I_n, and V_n clusters produced in the cascade. These initial concentrations were obtained from MD results by dividing—for each defect type and size—the number of defects by the volume of the simulation box. It is important to note that this averaging implicitly wipes out the existing spatial correlations between defects and implies that clusters are considered to be homogeneously distributed in space in the RT model. Rate equations (17)–(25) were solved using the partial differential equation solver PROMIS 1.5.[38] In Fig. 4, the evolution of the total number of defects predicted by kMC and RT is reported for an irradiation dose of 10^{-6} dpa. The differences between the two models are very small and it seems that the evolution of the defect population can be reproduced by the RT model.

The corresponding recovery curves obtained from the derivative with temperature and presented in Fig. 5 reveal that, in fact, there are some significant differences between RT and kMC calculations. As expected, the RT model does not predict stage I_{D2} resulting from correlated recombinations between interstitials and vacancies around $T=115$ K. Stages I_E and II corresponding to the migration of *I* and I_2 are predicted by the RT model, although their position is slightly shifted toward higher temperatures. This is again due to a dose effect. The recovery peak predicted by the kMC model at $T=231$ K (III_A) is also not accounted for by the RT model. However, interestingly, the amplitudes and positions of all

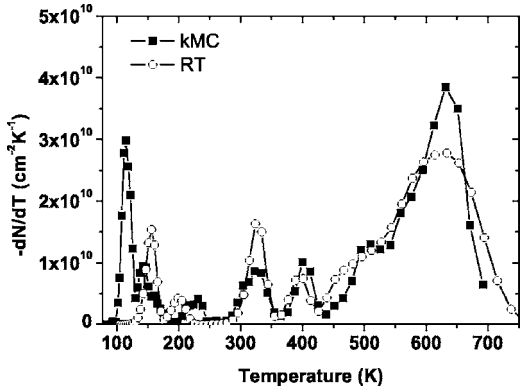

FIG. 5. Recovery stages predicted by kMC (■) and RT (○) models for a 30 keV Fe irradiation for a dose of 10^{-6} dpa.

subsequent peaks predicted by the kMC are well reproduced by the RT model. It seems, under these conditions, that the contribution of spatially correlated recombinations is small, and therefore the lack of correlations in RT does not significantly affect the results obtained at high temperatures.

In Fig. 6, the recovery curves obtained by the kMC and RT models are presented for a higher dose, 10^{-4} dpa. As in the lower-dose case, there are discrepancies at low temperature between RT and kMC due to the lack of spatial correlations, but there is good agreement at high temperature between the two models that seems to improve with increasing dose. The intensities and positions of the peaks for temperatures higher than 300 K are very well reproduced by the RT model. Notice that for this dose, the RT model predicts a peak at $T=264$ K. The origin of this peak will be discussed in the next section. It is interesting to point out that, unlike in the case of electron irradiation, the increase in dose does not shift the position of the different peaks with temperature. In particular, we can see that stage I_E does not change with dose, in agreement with neutron irradiation experiments carried out by Matsui *et al.*[37]

In addition, in Fig. 7 we report the evolution of the I_n and V_n cluster mean size calculated by both methods, for a dose of 10^{-4} dpa. In comparison to reference kMC simulations, RT model reproduces well the growth of interstitial and vacancy clusters in the whole temperature range.

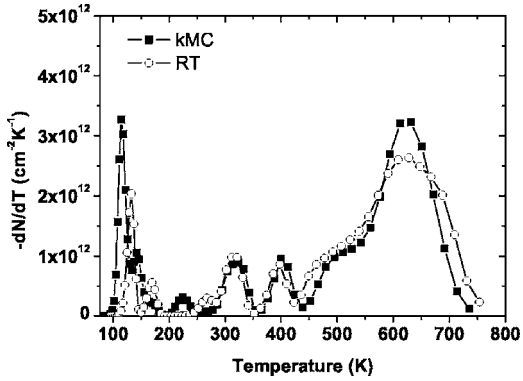

FIG. 6. Recovery stages predicted by kMC (■) and RT (○) models for a 30 keV Fe irradiation for a dose of 10^{-4} dpa.

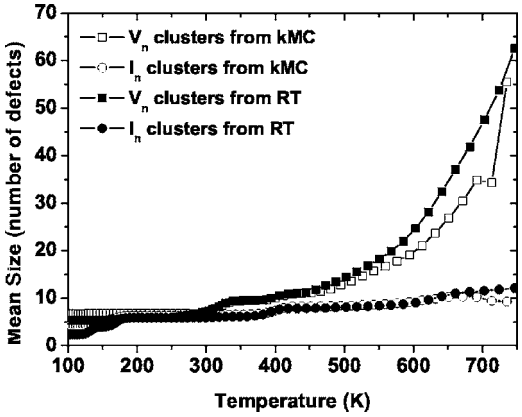

FIG. 7. Evolution of I_n and V_n cluster mean size during isochronal annealing for a dose of 10^{-4} dpa according to kMC (open symbols) and RT (full symbols) models.

VI. DISCUSSION

As we have seen in the previous section, when irradiation yields intracascade clustering, the defect recovery curve exhibits a more complex structure than in electron irradiation conditions, where only Frenkel pairs are produced. This indicates that additional recombination mechanisms govern the evolution of defects. Thus, according to the model described in Sec. IV, kMC calculations show that in addition to stages I_{D2}, I_E, II, and III observed under electron irradiation, three new recovery peaks can be expected for a 30 keV Fe irradiation in Fe. Clearly, these peaks (III_A, IV_A, and IV_B) are related to the intracascade clustering that occurs during ion irradiation. In this section, we shall discuss the recombination mechanisms responsible for these recovery peaks.

A. Peak III_A

The first recovery peak associated with intracascade clustering is centered at $T=231$ K, according to kMC results shown in Fig. 6. To determine the recombination mechanism responsible for this peak, in Fig. 8 we reported the evolution of different defect populations obtained with the kMC model for an irradiation dose of 10^{-4} dpa. As one can see, peak III_A

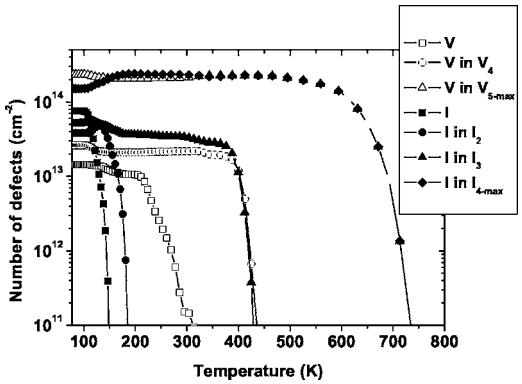

FIG. 8. Evolution of different vacancy (open symbols) and interstitial (full symbols) populations during isochronal annealing obtained by kMC calculations for an irradiation dose of 10^{-4} dpa.

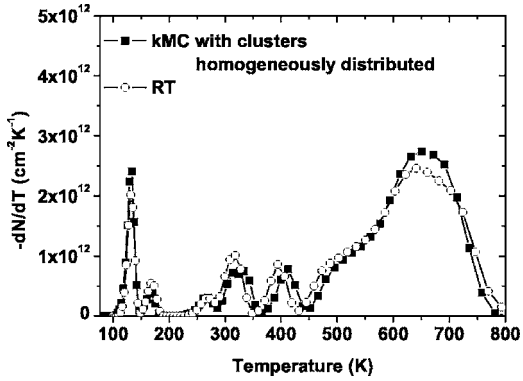

FIG. 9. Comparison between recovery curves for an irradiation dose of 10^{-4} dpa obtained with the kMC model assuming all clusters are homogeneously distributed (■) and the RT (○) model.

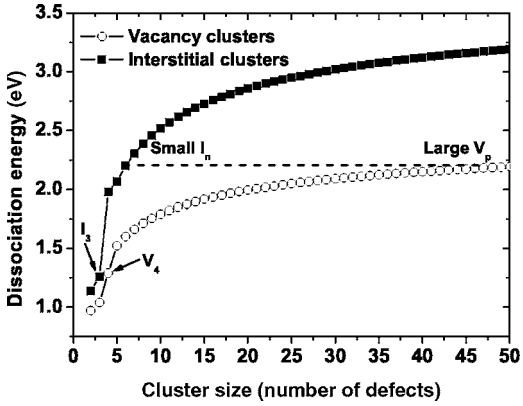

FIG. 10. Dissociation energies of I_n and V_n clusters in Fe. The dissociation energy is defined as the sum of the binding energy and the migration energy of the point defect released.

appears when the population of mobile vacancies drops. Since all I and I_2 have already recombined at this temperature, as shown in Fig. 8, this seems to indicate that peak III_A is due to the annihilation of migrating vacancies with immobile interstitial clusters $I_{n\geqslant 3}$. However, this peak is not observed in the recovery curve calculated by the RT model. Instead, a peak at $T=264$ K is seen in the RT calculations, i.e., at a higher temperature.

This strongly suggests that the recovery peak III_A predicted by kMC calculations results from recombinations of close correlated V-$I_{n\geqslant 3}$ arrangements that form during the collision cascade. To confirm this hypothesis, kMC simulations were performed with, as initial conditions, the defects created during irradiation homogeneously and randomly distributed in space, i.e., without spatial correlations. Results are shown in Fig. 9 and compared to RT simulations. We can see that in that case, kMC and RT results almost overlap, as it was observed by Rottler *et al.*[18] in similar conditions. Now, both kMC and RT models show a peak at $T=264$ K with the same intensity and none of them show peak at 231 K. Thus, peak III_A seen at $T=231$ K in the kMC calculations is due to the recombination of correlated V-$I_{n\geqslant 3}$ arrangements that form in the cascade during irradiation, whereas the one observed at $T=264$ K in the RT model is due to uncorrelated recombinations between V and $I_{n\geqslant 3}$. In this last case, i.e., when defects are not correlated, the peak appears at a higher temperature since vacancies must migrate over a larger mean distance to find an interstitial cluster.

B. Peak IV_A

Next, recovery peak (IV_A) related to the intracascade clustering is predicted by our model to appear at $T=400$ K, according to Figs. 5 and 6. Figure 8 shows that peak IV_A corresponds to the fast decay of I_3 and V_4 cluster populations. The fact that these clusters have similar dissociation energies—1.26 eV for I_3 against 1.29 eV for V_4—as can be seen in Fig. 10, implies that they must dissociate at similar rates. This strongly suggests that the recovery peak IV_A results from a double annihilation mechanism. In this scenario, I_3 clusters dissociate through the reaction $I_3 \rightarrow I_2 + I$, which then may annihilate with vacancy clusters. At the same temperature, V_4 clusters dissociate following $V_4 \rightarrow V_3 + V$. The vacancies released in this reaction may then recombine with interstitial-type defects, while in turn, V_3 clusters, which are less stable than V_4, dissociate through $V_3 \rightarrow V_2 + V$. Again, the vacancies released in this reaction may react with interstitial clusters. Finally, divacancy clusters which are unstable at this temperature, release two vacancies that recombine with I_n clusters.

C. Peak IV_B

Figure 3 shows that last recovery peak related to intracascade clustering and predicted by the kinetic model presented in Sec. IV spreads from 450 to 700 K (peak IV_B). This stage was observed by Takaki *et al.*[1] in this temperature range only at high electron irradiation doses and is often called stage IV. The authors attributed this stage to the dissolution of large clusters. In the case of intracascade clustering, our simulations also support this view and enable us to identify the atomistic mechanisms responsible for this recovery stage. Figure 7, in which the mean size evolution of clusters is reported, reveals that I_n and V_n clusters formed in the cascade grow in size in the 77–700 K temperature interval. In particular, we can see that the mean size of vacancy clusters is significantly larger than that of interstitial ones, since self-interstitial clusters are considered immobile in these calculations and vacancy clusters are less stable than self-interstitial clusters. Thus, the recovery peak IV_B is associated with the dissolution of large clusters. From Fig. 10, it is interesting to note that small interstitial clusters have similar dissociation energies compared to large vacancy voids. This means that at a given temperature, these two type of defects must release point defects at a similar rate. Therefore, we propose that recovery peak IV_B spreading from 450 to 700 K is due to the simultaneous dissociation of small interstitial and large vacancy clusters. In this double recombination mechanism, large V_n clusters release free vacancies through $V_n \rightarrow V_{n-1} + V$, which then annihilate with interstitial clusters following reaction (15). At the same time, interstitials dissociate from small I_n clusters through $I_n \rightarrow I_{n-1} + I$ and recombine with large vacancy clusters accord-

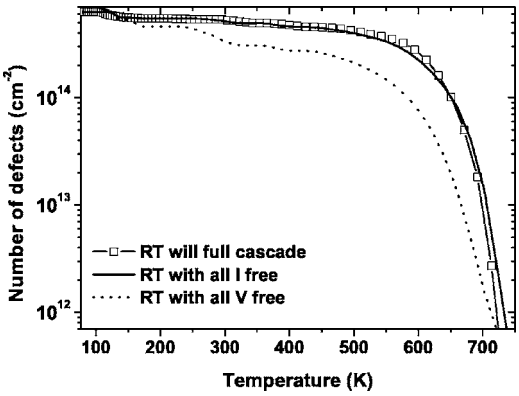

FIG. 11. Influence of the initial formation of interstitial and vacancy clusters in the cascade on the kinetics of defect annealing for a dose of 10^{-4} dpa.

ing to reaction (16). These dissociation-recombination reactions continue until all clusters have dissolved.

D. Influence of initial defect size distributions on damage evolution

In this section, we study in more detail the role of each defect distribution (I_n and V_n) created during irradiation on damage evolution. To do so, RT simulations were performed with various initial conditions. (i) Only vacancy clusters form during cascade collisions. All interstitial defects are considered to be single self-interstitials free to diffuse. (ii) Only interstitial clusters are created during irradiation. Vacancies remain as isolated defects. (iii) All the clusters are taken into account in the initial conditions. Figure 11 shows the evolution of the defect population obtained for each initial condition for an irradiation dose of 10^{-4} dpa. When initial conditions (i) are considered, results obtained are similar to those obtained with the full cascade information, as shown in Fig. 11. In contrast, when initial conditions (ii) are used, the model highly underestimates the defect population. This discrepancy can be explained by the difference in migration energies of I and V. Indeed, self-interstitials diffuse much faster than vacancies, with a migration energy of 0.34 eV against 0.67 eV, respectively. Hence, after irradiation, self-interstitials may agglomerate into I_n clusters at low temperature, which does not affect the subsequent evolution of defects. This situation corresponds to initial conditions (i). On the other hand, when all vacancies are assumed to be free to migrate after irradiation, they may recombine with highly mobile self-interstitials, di-interstitials, and interstitials released from I_n clusters before they agglomerate into V_n clusters. These recombinations strongly affect defect populations. Thus, to properly predict damage evolution after cascade damage, it is crucial to properly determine the initial vacancy cluster size distribution created during irradiation. On the other hand, the initial size distribution of interstitial defects seems to play a minor role on the damage evolution. All self-interstitials created during irradiation can be considered as mobile since they agglomerate in the very early stages of annealing.

VII. CONCLUSIONS

Thermal evolution of damage produced in Fe by 30 keV recoils was studied using two simulation approaches, kinetic monte carlo and rate theory. kMC simulations showed that when clusters form during irradiation, the evolution of defects strongly differs from that obtained under electron irradiation conditions, where only Frenkel pairs are produced. Within the kinetic model used in this work, simulated defect recovery curves show that additional recombination peaks should be expected in the presence of intracascade clustering. Detailed kMC and RT simulations showed that some of these recovery peaks are related to correlated recombinations between defects. In particular, we show that when there is a heterogeneous distribution of defects, it is possible to observe correlated recombinations between vacancies and self-interstitial clusters. These correlated recombinations cannot be reproduced with a RT model, and therefore kMC and RT differ at low temperature. However, for the conditions presented here, the contribution of correlated recombinations is very small and therefore no significant differences are observed at high temperature between RT and kMC calculations. Since RT models require small computational resources, they represent thus an attractive alternative to kMC approach to predict defect evolution under these conditions.

The peaks obtained by these models at two different doses have been analyzed in detail. In particular, simulation results revealed that the first peak, seen at $T=231$ K (III_A), is due to correlated recombinations of V-$I_{n\geq 3}$ arrangements formed during irradiation. The next recovery peak, predicted at $T=400$ K (IV_A), was found to result from the simultaneous dissociation of I_3 and V_4 clusters that have similar dissociation energies. Similarly, the concomitant dissolution of small I_n and large V_n clusters was found to be responsible for the recovery peak IV_B, spreading from 400 to 750 K. Additional RT simulations showed that the initial size distribution of vacancy clusters created during irradiation in Fe plays a crucial role in the prediction of the subsequent defect evolution. On the other hand, we found that the evolution of defects in Fe after ion irradiation is not affected if the initial formation of interstitial clusters in the cascade is neglected. Simulations show that all self-interstitials formed by collision cascades can be considered as free to migrate. This was explained by the fact that self-interstitials diffuse at low temperature and agglomerate into I_n clusters at the very beginning of annealing.

Further work will include the effect of damage accumulation under continuum irradiation and the effect of spatial correlations as well as dose rate and temperature.

ACKNOWLEDGMENTS

C.J.O. acknowledges the European Commission for financial support through the TOOLSPIE Euratom project FI60-012648. M.J.C. thanks the Spanish MEC for support under the Ramon y Cajal program. Part of this work was carried out within the PERFECT (IP FI60-CT-2003-508840) project funded by the EC. Molecular-dynamics simulations were

performed on the Mare Nostrum computer in the Barcelona Supercomputing Center. kMC calculations were performed on the Beowulf cluster built by GuiriSystems at Departamento de Física Aplicada from University of Alicante.

*Electronic address: christophe.ortiz@ua.es

[1] S. Takaki, J. Fuss, H. K. U. Dedek, and H. Schultz, Radiat. Eff. **79**, 87 (1983).
[2] R. S. Averback and T. D. de la Rubia, in *Solid State Physics*, edited by F. Spaepen and H. Ehrenreich (Academic, New York, 1998), Vol. 51, pp. 281–402.
[3] D. J. Bacon, F. Gao, and Y. Osetsky, J. Nucl. Mater. **276**, 1 (2000).
[4] C. Domain and C. S. Becquart, Phys. Rev. B **65**, 024103 (2001).
[5] C. C. Fu, F. Willaime, and P. Ordejon, Phys. Rev. Lett. **92**, 175503 (2004).
[6] H. L. Heinisch, Radiat. Eff. Defects Solids **113**, 53 (1990).
[7] M. J. Caturla, N. Soneda, E. Alonso, B. D. Wirth, T. D. de la Rubia, and J. M. Perlado, J. Nucl. Mater. **276**, 13 (2000).
[8] C. Domain, C. S. Becquart, and L. Malerba, J. Nucl. Mater. **335**, 121 (2004).
[9] C. C. Fu, J. D. Torre, F. Willaime, J.-L. Bocquet, and A. Barbu, Nat. Mater. **4**, 68 (2005).
[10] A. H. Duparc, C. Moingeon, N. Smetniansky-de-Grande, and A. Barbu, J. Nucl. Mater. **302**, 143 (2002).
[11] B. D. Wirth, M. J. Caturla, T. D. de la Rubia, T. Khraishi, and H. Zbib, Nucl. Instrum. Methods Phys. Res. B **180**, 23 (2001).
[12] H. Trinkaus, B. N. Singh, and S. I. Golubov, J. Nucl. Mater. **283-287**, 89 (2000).
[13] L. K. Mansur, E. H. Lee, P. J. Maziasz, and A. P. Rowcliffe, J. Nucl. Mater. **633**, 141 (1986).
[14] S. I. Golubov, B. N. Singh, and H. Trinkaus, J. Nucl. Mater. **276**, 78 (2000).
[15] C. H. Woo and B. N. Singh, Philos. Mag. A **65**, 889 (1992).
[16] M. P. Surh, J. B. Sturgeon, and W. G. Wolfer, J. Nucl. Mater. **325**, 44 (2004).
[17] C. J. Ortiz, P. Pichler, T. Fühner, F. Cristiano, B. Colombeau, N. E. B. Cowern, and A. Claverie, J. Appl. Phys. **96**, 4866 (2004).
[18] J. Rottler, D. J. Srolovitz, and R. Car, Phys. Rev. B **71**, 064109 (2005).
[19] A. A. Semenov and C. H. Woo, J. Nucl. Mater. **233-237**, 1045 (1996).
[20] A. A. Semenov and C. H. Woo, Appl. Phys. A: Mater. Sci. Process. **69**, 445 (1999).
[21] C. H. Woo, J. Comput.-Aided Mater. Des. **6**, 247 (1999).
[22] J. Dalla Torre, C. C. Fu, F. Willaime, A. Barbu, and J.-L. Bocquet, J. Nucl. Mater. **352**, 42 (2006).
[23] J. R. Beeler and D. G. Besco, J. Appl. Phys. **34**, 2873 (1963).
[24] D. G. Doran, Radiat. Eff. **2**, 249 (1970).
[25] J. Bronsted, Z. Phys. Chem., Stoechiom. Verwandtschaftsl. **102**, 169 (1922).
[26] M. von Smoluchowski, Z. Phys. Chem., Stoechiom. Verwandtschaftsl. **92**, 129 (1917).
[27] T. R. Waite, Phys. Rev. **107**, 463 (1957).
[28] T. R. Waite, Phys. Rev. **107**, 471 (1957).
[29] D. Peak and J. W. Corbett, Phys. Rev. B **5**, 1226 (1972).
[30] N. Soneda and T. D. de la Rubia, Philos. Mag. A **78**, 995 (1998).
[31] F. Maury, M. Biget, P. Vajda, A. Lucasson, and P. Lucasson, Phys. Rev. B **14**, 5303 (1976).
[32] R. E. Stoller, in *Effects of Radiation on Materials*, 16th International Symposium, edited by A. S. Kumar, D. S. Gelles, R. K. Nanstad, and E. A. Little (ASTM, Philadelphia, PA, 1993), Vol. 51, p. 34.
[33] G. J. Ackland, D. J. Bacon, A. F. Calder, and T. Harry, Philos. Mag. A **75**, 713 (1997).
[34] M. I. Mendelev, S. Han, D. J. Srolovitz, G. J. Ackland, D. Y. Sun, and M. Asta, Philos. Mag. **83**, 3977 (2003).
[35] S. L. Dudarev and P. M. Derlet, J. Phys.: Condens. Matter **17**, 7097 (2005).
[36] M. D. Johnson, M. J. Caturla, and T. D. de la Rubia, J. Appl. Phys. **84**, 1963 (1998).
[37] H. Matsui, S. Takehana, and M. W. Guinan, J. Nucl. Mater. **155-157**, 1284 (1988).
[38] P. Pichler, W. Jungling, S. Selberherr, E. Guerrero, and H. W. Pötzl, IEEE Trans. Comput.-Aided Des. **4**, 384 (1985).